Constraints on DBI dark energy with chameleon mechanism

Burin Gumjudpai,[1, *] Nandan Roy,[1, †] and John Ward[2, ‡]

[1]NAS, Centre for Theoretical Physics & Natural Philosophy

Mahidol University, Nakhonsawan Campus, Phayuha Khiri, Nakhon Sawan, Thailand 60130

[2]*Arbutus Studios, West Broadway, Vancouver, BC, Canada, V6K0B1*

(Dated: August 8, 2025)

In this work, we investigate the Dirac–Born–Infeld chameleon scalar field model in light of the latest cosmological observations, analyzing the model both with the incorporation of the chameleon mechanism and without it. Results from current cosmological observations, such as Pantheon Plus, DES Y5, DESI DR2, and the compressed Planck likelihood, are used to constrain the model. We consider the AdS throat in the form of $f(\phi) = \lambda/\phi^4$ and a potential $V(\phi) = m_0^2\phi^2 + m_1^2\phi^4$. One interesting finding from our analysis is that, without the chameleon mechanism, the mean value of $m_1 \simeq 0$ indicates the self-interaction of the DBI field could potentially be negligible. Constraints on the potential parameters do not appear when considering the chameleon mechanism, but the warp parameter and chameleon coupling parameter are forced to satisfy $\eta \geq 0$ and $\beta \leq 0$. Different choices of β render the same background cosmological parameters. The equation of state w_{DE} resides more in the quintessence region in the past. There is no phantom crossing in this model under our assumption of the warp throat and potential. By computing the ΔAIC relative to the ΛCDM model, we study statistical model comparison. The model as a candidate of dynamical dark energy is observationally viable at the cosmological background level.

I. INTRODUCTION

The simple solution to the problem of the present acceleration of the universe [1] is to postulate the existence of a vacuum energy or cosmological constant that agrees with all the current observational bounds [2]. However, the vacuum energy needs to be fine-tuned to a small value on the other side to accommodate the present acceleration [3] and apart from this the vacuum energy or the cosmological constant must overcome the discrepancies coming from very recent cosmological observations [4]. A discordance between the measurement of the Hubble parameter from the early universe data, for example, Planck [2], BAO [5], DES [6] etc. and the late-time observations like SH0ES [7, 8], HOLiCOW [9], CCHP [10] etc. is of the order of 5σ. Recent results derived from the Dark Energy Spectroscopic Instrument (DESI) [11–15] and the Year 5 supernovae dataset from the Dark Energy Survey (DES) [16] indicate that at low redshift, both the BAO and supernovae data might not favor the conventional ΛCDM model, suggesting that dark energy could be dynamical in nature. These discrepancies between the observations and the theoretical problems faced by the cosmological constant, and the discordance in the value of the Hubble parameter, lead us to explore different alternative ideas for the cause of the accelerated expansion of the universe [17–20].

Light scalar fields are frequently explored as possible contributors to the cosmic accelerating expansion [17, 20]. Various scalar field models, such as quintessence,

k-essence and phantom field, have been developed to describe this phenomenon [19, 21]. In these scenarios, cosmic acceleration arises from the dynamics of a scalar field evolving under a potential, leading to an effective negative pressure that drives expansion [17, 20, 22–26].

Although the introduction of scalar fields can help us to explain some outstanding problems in cosmology, they also create problems related to the local astronomical observations. Generally, the scalar field or the moduli considered in the cosmological models are massless. To be compatible with the local astronomical test, the masses of these scalar fields must be of the order of the Hubble scale or less. These light scalar fields, if coupled to matter, would have fifth-force gravitational strength which could produce unacceptably large violation of the Equivalence Principle in the solar system or at smaller scales. Hence, a screening mechanism for the fifth force is needed in order for the theory to pass local experimental constraints, but allowing GR modification at large scales (see, e.g. [27] for review).

A screening mechanism called the chameleon mechanism can remove the mentioned problems of the light scalar field, that is, suppress the local fifth force effect [28]. In the chameleon mechanism, the mass of the scalar field depends on its ambient matter density. Specifically, the mass of the scalar field (the chameleon field) decreases in regions of low matter density, while it becomes larger in high-density regions. For a heavy chameleon field, the associated Compton wavelength is less, consequently the force mediated by the field becomes short-ranged [29–33]. In the early universe, the chameleon field faces significant challenges. As massive particle species become non-relativistic during the radiation era, the field experiences *kicks* that induce rapid motion [34–36]. This can lead to a *surfer* solution, where the field, moving at high velocity, tracks the minimum of its effective potential

at constant Jordan-frame temperature. Upon reflection from the steep potential wall, the field's kinetic energy drops to zero, triggering sharp variations in its effective mass and exciting high-energy modes. As a result, classical evolution breaks down, undermining the chameleon model's predictability during the Big Bang Nucleosynthesis epoch [37, 38].

It has been shown that incorporating Dirac–Born–Infeld (DBI) corrections into chameleon models can mitigate the adverse effects of such *kicks* in the early universe. The presence of the DBI term weakens the effective coupling between the chameleon field and matter preventing the field to reach very high velocity, thereby protecting the field from excitation of high-energy modes [39]. Hence introducing of the DBI field as the chameleon can avoid the surfer solution hence alleviating or solving the problem caused by chameleon at the Big Bang Nucleosynthesis.

The DBI models were first used in cosmology to explain inflation. The idea comes from string theory in which the open string in Dp-branes can be dynamical and drive inflation at the early epoch. The inflation field is dual to the radial coordinate of a $D3$ brane moving in a throat of warped compactified space. The motion of the $D3$ brane is limited in its speed, and it is affected by the speed of the brane and the throat's warp factor, which could be of AdS_5 type[40–48]. The kinetic part of the DBI action is a non-standard term and is a function of the scalar field, and the potential is identified with the compact manifold's local geometry, which is traversed to the $D3$-brane. In the context of inflation, the DBI field was initially suspected to generate excessively large non-Gaussianities. However, it was later shown that the simplest DBI inflationary models yield predictions similar to those of the standard scalar-field slow-roll scenarios [49–53]. Subsequently, DBI models have been explored as potential candidates for dark energy [48, 54–59]. More recently, the DBI field has also been proposed as a possible candidate for dark matter, particularly in relation to addressing the S_8 tension [60].

In this work, we consider the DBI scalar field as the dark energy component of the universe and employ current cosmological observations, including Supernovae, Baryon Acoustic Oscillations (BAO), and Cosmic Microwave Background (CMB) data, to constrain the model parameters. We examine two distinct scenarios: the DBI field without the chameleon mechanism and the DBI field incorporating the chameleon mechanism.

The manuscript is organized as follows. In Section III, we present the derivation of the field equations from the DBI action. Section IV describes the observational data sets used in this work. The results of our analysis are discussed in Section V, and we summarize our conclusions in Section VI.

II. DBI ACTION WITH CHAMELEON MECHANISM

Considering the action for a BPS $D3$-brane localized in a warped compacification of type IIB string theory. We will also assume the existence of a matter sector coupled to the world-volume theory of the brane. The resulting action can then be written in the form [48]

$$
S_\phi = \\
-\int \mathrm{d}^4 x \sqrt{-g} \left(T(\phi) \left(W(\phi) \sqrt{1 - \frac{2X}{T}} - 1 \right) + V(\phi) \right)
\tag{1}
$$

This is the generalised Dirac-Born-Infeld (DBI) action where

$$
X \equiv -\frac{1}{2} g^{\mu\nu} \partial_\mu \phi \partial_\nu \phi = -\frac{1}{2}(\nabla \phi)^2
$$
$$
\Gamma \equiv \sqrt{1 + \frac{(\nabla \phi)^2}{T}}
$$

and as we consider here $W = 1$, a usual DBI case. One can find that the action (1) reads

$$
S_\phi = \int \mathrm{d}^4 x \sqrt{-g} \Big[-T(\Gamma - 1) - V \Big]
\tag{2}
$$

where $T = 1/f(\phi)$ and $f(\phi)$ is warped factor (for AdS throat, $f(\phi) = \lambda/\phi^4$). We define the DBI Lagrangian density as $\mathcal{L}_\phi \equiv -T(\Gamma - 1) - V$. In this system the total action is of the Einstein-Hilbert, matter field and the DBI scalar field terms,

$$
S = \int \mathrm{d}^4 x \Big\{ \mathcal{L}_{\mathrm{EH}} + \mathcal{L}_{\mathrm{m}}(\psi_\mu, \tilde{g}_{\mu\nu}) \\
+ \sqrt{-g} \Big[-T(\Gamma - 1) - V \Big] \Big\},
\tag{3}
$$

Hence $\mathcal{L}_{\mathrm{EH}} \equiv (M_{\mathrm{Pl}}^2/2)\sqrt{-g}\mathcal{R}$, $\mathcal{L}_\phi = \sqrt{-g}\left[-T(\Gamma - 1) - V \right]$, where $\mathcal{R}$ is the Ricci-scalar, M_{Pl} is reduced Planck mass, and ψ_{m} is a matter field. We define Jordan frame metric

$$
\tilde{g}_{\mu\nu} = e^{2\beta\phi/M_{\mathrm{Pl}}} g_{\mu\nu}.
\tag{4}
$$

The kinetic term for the scalar field ϕ is encoded in the DBI-part of the action $(-T(\Gamma - 1))$. Matter field term can be varied independently to have $\delta S_{\mathrm{m}} = 0$, into the total action. Symbol $'$ denotes $\mathrm{d}/\mathrm{d}\phi$. Following details in the appendix, we obtain the DBI equation of motion,

$$
\frac{\Box^2 \phi}{\Gamma} - \frac{T'}{2\Gamma}(\Gamma - 1)^2 - \frac{1}{\Gamma^2} g^{\mu\nu}(\partial_\mu \phi)(\partial_\nu \Gamma) \\
= V' - \frac{\mathcal{L}'_m}{\sqrt{-g}}
\tag{5}
$$

The last term is the matter Lagrangian density. With coupling between the scalar field to the metric via the

equation (4)-the chameleon mechanism, the matter Lagrangian reads

$$\mathcal{L}'_{\mathrm{m}} \; = \; -\sqrt{-g}\,\frac{\beta}{M_{\mathrm{Pl}}}\,\rho(1-3w)\,e^{\beta(1-3w)\phi/M_{\mathrm{Pl}}} \qquad (6)$$

where w is equation of state parameter of barotropic fluid, i.e. matter and radiation. Considering dust fluid ($w = 0$), the full DBI field equation of motion with chameleon mechanism is hence

$$\begin{aligned}\frac{\Box^2\phi}{\Gamma} - \frac{T'}{2\Gamma}\,(\Gamma-1)^2 &- \frac{1}{\Gamma^2}\,g^{\mu\nu}(\partial_\mu\phi)(\partial_\nu\Gamma) \\ &= \; V' + \frac{\beta}{M_{\mathrm{Pl}}}\,\rho\,e^{\beta\phi/M_{\mathrm{Pl}}}\end{aligned} \qquad (7)$$

The last term on the right hand side is proportional to the energy density of the matter sector. One finds this expression by noting that variation of the matter Lagrangian yields a term proportional to $\tilde{T}^{\mu\nu}\tilde{g}_{\mu\nu}$ which for an isotropic fluid will be of the form $-(1 - 3w)\tilde{\rho}$ in the Jordan frame. In Einstein frame we see that $\rho = \tilde{\rho}\,e^{3(1+w)\beta\phi/M_{\mathrm{Pl}}}$. The effective potential is therefore defined as

$$V'_{\mathrm{eff}} \; \equiv \; V' + \frac{\beta\rho}{M_{\mathrm{Pl}}}e^{\beta\phi/M_{\mathrm{Pl}}}. \qquad (8)$$

The field equation (7) can be treated as temporal dependent and radial dependent. Their solutions will be investigated here.

Assuming that the metric is flat FRW and that the scalar field is homogeneous, i.e. only-time dependent, the equation of motion therefore reduces to

$$\begin{aligned}-\ddot{\phi} - \Gamma^2\,3H\dot{\phi} &+ \frac{T'}{2}\,\left(1 - 3\Gamma^2 + 2\Gamma^3\right) \\ &= \; \left(V' + \frac{\beta}{M_{\mathrm{Pl}}}\,\rho\,e^{\beta\phi/M_{\mathrm{Pl}}}\right)\Gamma^3\end{aligned} \qquad (9)$$

where here $\Gamma = (1 - \dot{\phi}^2/T)^{1/2}$.

The density and the pressure of the DBI field can be written as;

$$p_\phi \; = \; T(\phi)\Gamma(\phi)[1/\Gamma(\phi) - 1] - V(\phi)\,, \qquad (10\mathrm{a})$$
$$\rho_\phi \; = \; T(\phi)[1/\Gamma(\phi) - 1] + V(\phi)\,. \qquad (10\mathrm{b})$$

To determine the potential governing the dynamics of the DBI scalar field in our dark energy scenario, the action (1) must remain invariant under a group of internal symmetries. In particular, for the action to be symmetric under the transformation $\phi \to -\phi$, the potential $V(\phi)$ must be an even function. Following previous studies [54, 59], we adopt the form

$$V(\phi) = m_0^2\phi^2 + m_1^2\phi^4, \qquad (11)$$

where m_0 and m_1 are constant parameters. Here, m_0 represents the effective mass of the scalar field, while m_1

controls the strength of the self-interaction term. This potential structure naturally accommodates spontaneous symmetry breaking at an energy scale significantly higher than that of the present universe—a feature with important implications for theoretical cosmology [61].

For the DBI warp factor, we assume an anti–de Sitter (AdS) form,

$$f(\phi) = \frac{\lambda}{\phi^4}, \qquad (12)$$

where λ is a constant parameter governing the brane tension in the DBI framework.

III. OBSERVATIONAL DATA

In this section, we investigated the observational constraints on this model by comparing its predictions with current cosmological data, considering both cases: with and without the inclusion of the chameleon mechanism. For the Markov Chain Monte Carlo (MCMC) analysis, we employed the *emcee* package, while the posterior distributions resulting from our analysis were visualized using the GetDist plotting tool. A detailed description of the datasets used in this study is provided below.

A. Supernova Data

Type Ia supernovae are commonly utilized as standard candles due to their relatively uniform intrinsic luminosity [62, 63]. In this work, we have used the Pantheon Plus compilation of SN Ia data [64–67] and the DES Year 5 dataset [16]. These datasets are based on distinct photometric systems and selection criteria, and both provide measurements of the distance modulus μ across a wide range of redshifts.

B. DESI BAO Data

The density distribution of visible baryonic matter exhibits periodic fluctuations, known as baryon acoustic oscillations (BAO), which serve as important standard rulers for precise distance measurements in cosmology. In this work, we make use of the 2025 BAO observational data from the Dark Energy Spectroscopic Instrument (DESI-DR2), as presented in [11, 13].

The BAO measurements provide constraints on effective distance scales both along the line of sight and in the transverse direction. These are defined through the following relations.

For the line-of-sight direction, the comoving Hubble distance is given by:

$$\frac{D_H(z)}{r_d} = \frac{cr_d^{-1}}{H(z)}, \qquad (13)$$

where c is the speed of light, $H(z)$ is the Hubble parameter at redshift z, and r_d is the comoving sound horizon at the drag epoch.

For the transverse direction, the comoving angular diameter distance is expressed as:

$$\frac{D_M(z)}{r_d} \equiv \frac{c}{r_d} \int_0^z \frac{d\tilde{z}}{H(\tilde{z})} = \frac{c}{H_0 r_d} \int_0^z \frac{d\tilde{z}}{h(\tilde{z})}. \quad (14)$$

where H_0 is the present-day Hubble parameter and $h(z) = H(z)/H_0$.

The spherically averaged effective distance is defined as:

$$\frac{D_V(z)}{r_d} = \left[\frac{czr_d^{-3}d_L^2(z)}{H(z)(1+z)^2} \right]^{\frac{1}{3}}. \quad (15)$$

where $d_L(z)$ is the luminosity distance at redshift z.

where $d_L(z)$ denotes the luminosity distance. In this study, the sound horizon r_d is considered a free parameter and is determined through fitting to the observational data.

C. Compressed CMB Likelihood

We also utilize the Planck 2018 compressed likelihood, following the methodology presented in [68] (hereafter referred to as CMB). The compressed CMB prior provides a practical alternative to performing a full likelihood analysis of the complete Planck dataset, especially when exploring dark energy models that extend beyond the standard ΛCDM framework. This approach retains a comparable constraining power to the full Planck data while significantly reducing computational complexity.

The compressed likelihood incorporates the physical baryon density $\omega_b = \Omega_b h^2$, along with two key shift parameters: $l_A = (1 + z_*)\frac{\pi D_A(z_*)}{r_s(z_*)}$ and $\mathcal{R} = \sqrt{\Omega_M H_0^2} D_A(z_*)$, where z_* denotes the redshift at decoupling and D_A is the comoving angular diameter distance. It is important to note, however, that these priors may not fully capture the richness of the complete CMB power spectrum, particularly in models that exhibit significant deviations from ΛCDM. In such cases, systematic biases in the inferred cosmological parameters may arise [69, 70].

In this work, we consider the following three combinations of datasets to constrain our model:

1. *Pantheon Plus + CMB + DESI*

2. *DES Y5 + CMB + DESI*

3. *CMB + DESI*

IV. RESULTS

A. Without chameleon mechanism

Here, we study the DBI model without the chameleon mechanism, hence $\beta = 0$. We have considered a flat prior on the cosmological parameters $\Omega_{m0} : [0.26, 0.35], H_0 : [60, 75], r_d : [100, 170], w_b h^2 : [0.01, 0.03]$. The prior on the parameter related to the warp factor $\eta : [-5, 5]$, and on the potential parameters, $m_0 : [-10, 10], m_1 : [-20, 15]$. The prior on the current value of the ϕ and $\dot{\phi}$ has been considered to be $\phi_0 : [0.5, 1.5]$ and $\dot{\phi}_0 : [0.008, 0.012]$, ensuring that the MCMC analysis can proceed without encountering any stiffness during the exploration of the random walker.

The constraint derived from our analysis is presented in Table I, along with the mean and 1σ constraint level on the cosmological parameters. In Fig.1 we have shown the $1D$ and $2D$ triangular plot of the posterior distribution of $H_0, w_b h^2, \Omega_0, r_d$ obtained from our analysis. The red plot depicts the posteriors obtained for the *Pantheon Plus + CMB + DESI* data combination, the blue corresponds to the *DES Y5 + CMB + DESI*, and for the *CMB + DESI* it is shown in green. Figure 1 illustrates that the posteriors derived from each of these data sets exhibit remarkable consistency. The plot of the constraint obtained for the model parameters η, m_0, m_1 is shown in Fig.2. From our analysis, there is no constraint obtained on the scalar field throat parameter η. The parameter m_0 stays without constraints, whereas the obtained constraint on the mean value indicates $m_1 \simeq 0$. This suggests that the self-interaction of the DBI field could potentially be negligible.

In this work, we analysed the statistical performance of our proposed model in comparison to the standard ΛCDM cosmology. This evaluation was conducted using the minimum chi-squared statistic (χ_{min}^2), the chi-squared difference ($\Delta\chi^2$), and the difference in the Akaike Information Criterion (ΔAIC). Specifically, we computed the difference in minimum chi-squared values, $\Delta\chi_{min}^2$, between our model and the ΛCDM baseline, with the results presented in Table I. For each dataset considered, our model consistently achieved a better fit to the observational data than the ΛCDM framework.

As shown in Table I, for *Pantheon Plus + CMB + DESI*, the minimum chi-squared value is the lowest for the DBI model, yielding a difference of $\Delta\chi_{min}^2 = -16.826$ relative to ΛCDM. For *DES Y5 + CMB + DESI*, the difference is $\Delta\chi_{min}^2 = -22.436$, and for *CMB + DESI*, it is $\Delta\chi_{min}^2 = -20.813$. These results indicate a significantly improved fit to all three datasets when compared with the ΛCDM model.

The difference in AIC values is calculated using the following relation:

$$\Delta\text{AIC} = \chi_{min,\mathcal{M}}^2 - \chi_{min,\Lambda\text{CDM}}^2 + 2(N_\mathcal{M} - N_{\Lambda\text{CDM}}), \quad (16)$$

where $\mathcal{M}$ represents the model being tested, and $N_\mathcal{M}$ and $N_{\Lambda\text{CDM}}$ denote the number of parameters in models $\mathcal{M}$

Parameters	Pantheon Plus+CMB+DESI DR2		DES Y5+CMB+DESI DR2		CMB+DESI DR2	
	ΛCDM	DBI	ΛCDM	DBI	ΛCDM	DBI
Ω_{m0}	0.3178 ± 0.0058	0.3224 ± 0.0071	0.3195 ± 0.0058	0.3221 ± 0.0072	0.3129 ± 0.0060	0.3156 ± 0.0075
H_0	67.36 ± 0.42	67.03 ± 0.50	67.24 ± 0.42	67.06 ± 0.50	67.71 ± 0.44	67.52 ± 0.54
r_d	147.80 ± 0.43	148.76 ± 0.97	147.87 ± 0.43	148.76 ± 0.97	147.59 ± 0.44	148.40 ± 0.98
$\Omega_b h^2$	0.02237 ± 0.00013	0.02231 ± 0.00014	0.02234 ± 0.00013	0.02232 ± 0.00014	0.02242 ± 0.00013	0.02240 ± 0.00014
m_0	–	–	–	–	–	–
m_1	–	0.0 ± 2.0	–	0.0 ± 2.1	–	0.0 ± 2.1
χ^2_{min}	1794.038	1777.212	1714.250	1691.814	35.733	14.920
$\Delta\chi^2$	0	-16.826	0	-22.436	0	-20.813
ΔAIC	0	-6.826	0	-12.436	0	-10.813

TABLE I. Mean values of different cosmological parameters together with 68% constraints for the DBI model without the Chameleon mechanism. The result for the ΛCDM model is reported for comparison.

and ΛCDM, respectively. A negative ΔAIC relative to ΛCDM indicates that the model $\mathcal{M}$ is statistically preferred. The AIC criterion penalizes models with greater complexity, accounting for the number of free parameters. According to standard AIC interpretation, differences between -2 and -4 suggest weak evidence in favor of the model, differences between -4 and -7 indicate moderate support, and differences less than -10 imply strong support over ΛCDM.

Applying this framework to the datasets *Pantheon Plus + CMB + DESI*, *DES Y5 + CMB + DESI*, and *CMB + DESI*, we find ΔAIC values of -6.862, -12.436, and -10.813, respectively. These findings indicate that our model is preferred over ΛCDM across all datasets. The first two datasets provide moderate evidence, while the last two dataset combinations offer strong evidence in support of our model.

To test the evaluation of the cosmological parameters, we have plotted the evolution of the $H(z)$ against z in Fig. 3. The observational data from the cosmic chronometer data set has also been plotted for comparison. The choice of the parameter value for this plot is within the range of the posteriors obtained from the MCMC analysis. The plot of the evolution of the EoS of the scalar field for the same set of parameters is shown in the Fig.4. The EoS is very close to the $w_\phi = -1$ and shows a slight deviation from it at late times.

B. With chameleon mechanism

Here, we study the DBI model with the chameleon mechanism activated, hence $\beta \neq 0$. We have considered a flat prior on the cosmological parameters Ω_{m0} : $[0.26, 0.35]$, H_0 : $[60, 75]$, r_d : $[100, 170]$, $w_b h^2$: $[0.01, 0.03]$. The prior on the parameter related to the warp factor is η : $[-10, 10]$, the chameleon parameter β : $[-1.5, 0.3]$ and the priors on the potential parameters are m_0 : $[-10, 10]$, m_1 : $[-20, 15]$. The constraints obtained from our analysis are reported in Table II, along with the mean and 68% constraints on the cosmological parameters.

Figure 7 presents the one-dimensional and two-dimensional triangular plots of the posterior distributions
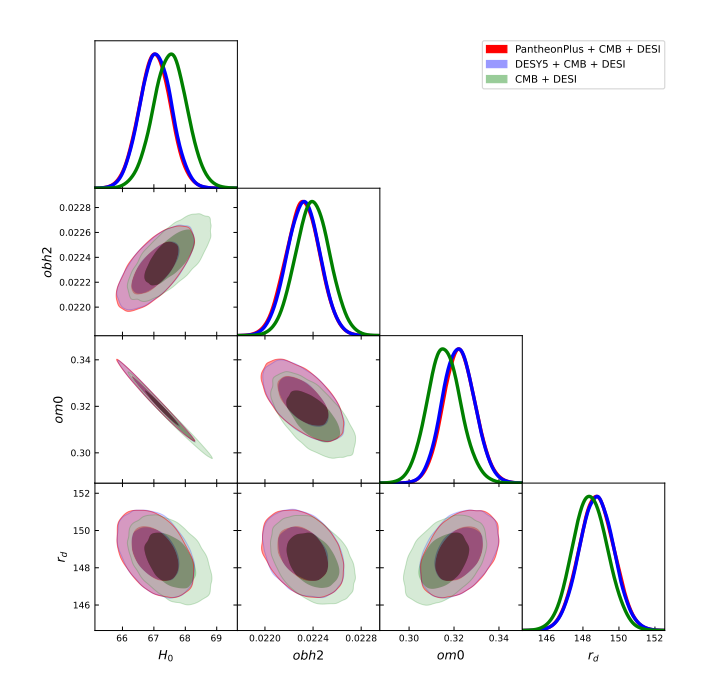

FIG. 1. The plot displays the triangular representation of the 1D and 2D posterior distributions for various cosmological parameters in the DBI model without the chameleon mechanism. The red contours correspond to results from *Pantheon Plus + CMB + DESI*, blue to *DES Y5 + CMB + DESI*, and green to *CMB + DESI*.

for $H_0, w_b h^2, \Omega_0, r_d$ as derived from our analysis. The posterior corresponding to the *Pantheon Plus + CMB + DESI* data set is illustrated in red, the *DES Y5 + CMB + DESI* in blue, and the *CMB + DESI* in green. This figure demonstrates the remarkable consistency of the posteriors across the different data sets. Meanwhile, Figure 8 displays the constraints for the model parameters η, β, m_0, m_1. Contrary to the previous case, in this scenario of the DBI field with the chameleon mechanism, there is a lower bound on the throat parameter (η). For this case $0 \leq \eta$. The chameleon coupling parameter β is constrained from above, and it has to be $\beta \leq 0$. Contrary to the previous case, here we do not find any constraint on

FIG. 4. Evolution of the EOS of the dark energy for the DBI model without the chameleon mechanism. For the choice of the parameters $m_0 = 0.1, m_1 = 10^{-4}, \eta = 1$ with the current value of the $\phi_0 \simeq 1, \dot{\phi}_0 \simeq 0.001$.
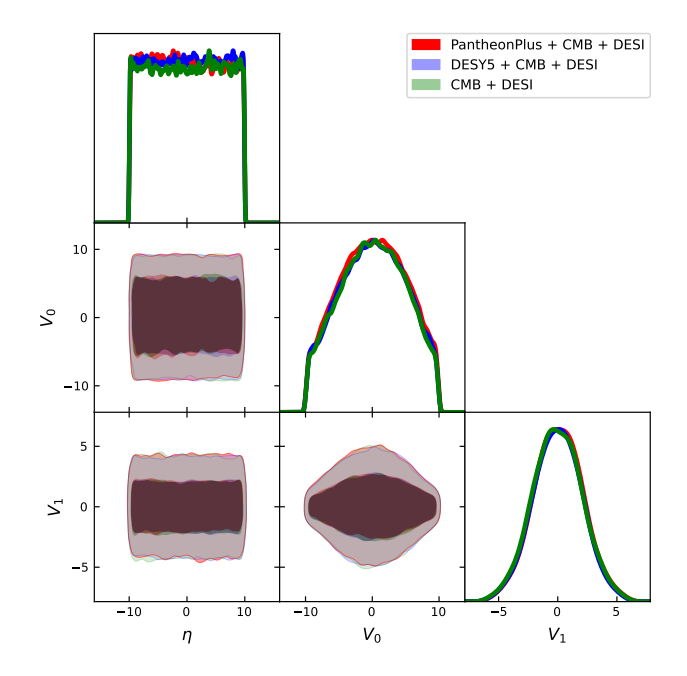
FIG. 2. The plot displays the triangular representation of the 1D and 2D posterior distributions for model parameters η, V_0, V_1 in the DBI model without the chameleon mechanism. The red contours correspond to results from *Pantheon Plus + CMB + DESI*, blue to *DES Y5 + CMB + DESI*, and green to *CMB + DESI*.
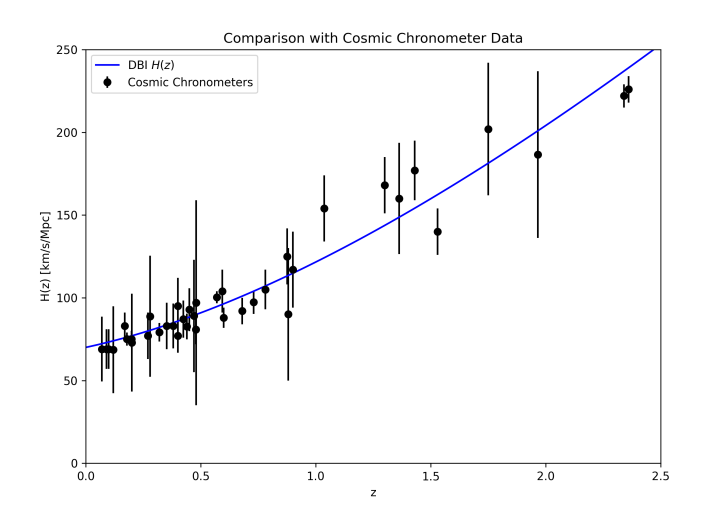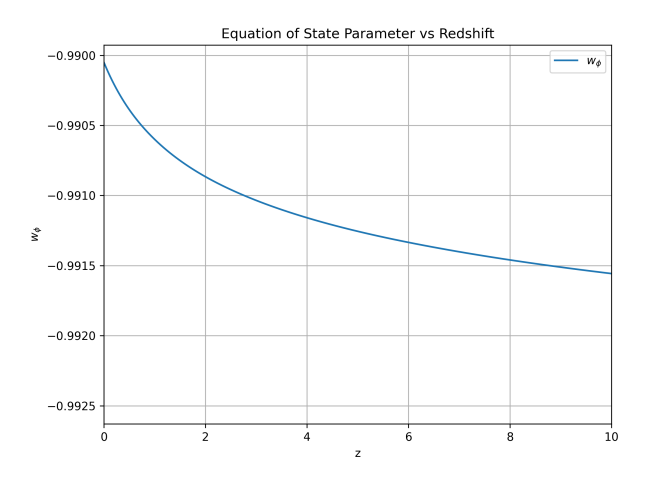

FIG. 3. Evolution of $H(z)$ versus redshift z for the DBI model without the chameleon mechanism. Data points from Cosmic Chronometer datasets are shown for comparison. For the choice of the parameters $m_0 = 0.1, m_1 = 10^{-4}, \eta = 1$ with the current value of the $\phi_0 \simeq 1, \dot{\phi}_0 \simeq 0.001$.

the scalar field parameters m_0 and m_1. For all three data combinations used here, the $\Delta\chi^2 < 0$ for this model when comparing with the ΛCDM model. For the *Pantheon Plus + CMB + DESI* combination, it is $\Delta\chi^2 = -21.939$, for the *DES Y5 + CMB + DESI* $\Delta\chi^2 = -22.382$ and for the *CMB + DESI* $\Delta\chi^2 = -20.869$. The calculation of

the ΔAIC shows a strong preference for this model for the last two data combinations, whereas the first data combination shows moderate preference for this model.

In order to evaluate cosmological parameters, we have illustrated the evolution of $H(z)$ as a function of z in Fig. 3. Additionally, observational data from the cosmic chronometer dataset is plotted for comparative purposes. The parameter values chosen for this visualization fall within the range of the posterior distributions derived from the MCMC analysis. Additionally, Fig. 4 illustrates the evolution of the scalar field's equation of state (EoS) utilizing the same set of parameters. The dark energy EoS exhibits quite a different behavior in this scenario compared to the situation where the chameleon mechanism is absent. With the chameleon mechanism in the distant past, the DBI field EoS was zero, mirroring the properties of matter; however, more recently, it has evolved to $w_\phi \approx -1$. This suggests that the DBI field with the chameleon mechanism could potentially offer a unified framework for describing both dark matter and dark energy, which we will explore in more detail in future studies.

V. CONCLUSION

The results from recent cosmological observations, such as DESI DR2 and DES Y5, suggest that dark energy might not be constant but rather evolving. Various proposals have been put forward for constructing dynamical dark energy models. In this work, we consider the Dirac-Born-Infeld (DBI) dark energy model and investigate its viability in light of current cosmological observations. We study this model both with and without the inclusion of the chameleon mechanism.

Parameters	Pantheon Plus+CMB+DESI DR2		DES Y5+CMB+DESI DR2		CMB+DESI DR2	
	ΛCDM	DBI + Chameleon	ΛCDM	DBI + Chameleon	ΛCDM	DBI + Chameleon
Ω_{m0}	0.3178 ± 0.0058	0.3228 ± 0.0074	0.3195 ± 0.0058	0.3221 ± 0.0072	0.3129 ± 0.0060	0.3156 ± 0.0075
H_0	67.36 ± 0.42	67.02 ± 0.50	67.24 ± 0.42	67.06 ± 0.50	67.71 ± 0.44	67.52 ± 0.54
r_d	147.80 ± 0.43	148.78 ± 0.98	147.87 ± 0.43	148.76 ± 0.97	147.59 ± 0.44	148.40 ± 0.98
$\Omega_b h^2$	0.02237 ± 0.00013	0.02235 ± 0.00019	0.02234 ± 0.00013	0.02232 ± 0.00014	0.02242 ± 0.00013	0.02240 ± 0.00014
η	$-$	≤ 0	$-$	≤ 0	$-$	≤ 0
β	$-$	$0 \leq$	$-$	$0 \leq$	$-$	$0 \leq$
χ^2_{min}	1794.038	1772.099	1714.250	1691.868	35.733	14.864
$\Delta\chi^2$	0	-21.939	0	-22.382	0	-20.869
ΔAIC	0	-9.939	0	-10.382	0	-8.869

TABLE II. Mean values of different cosmological parameters together with 68% constraints for the DBI model with the Chameleon mechanism. The result for the ΛCDM model is reported for comparison.
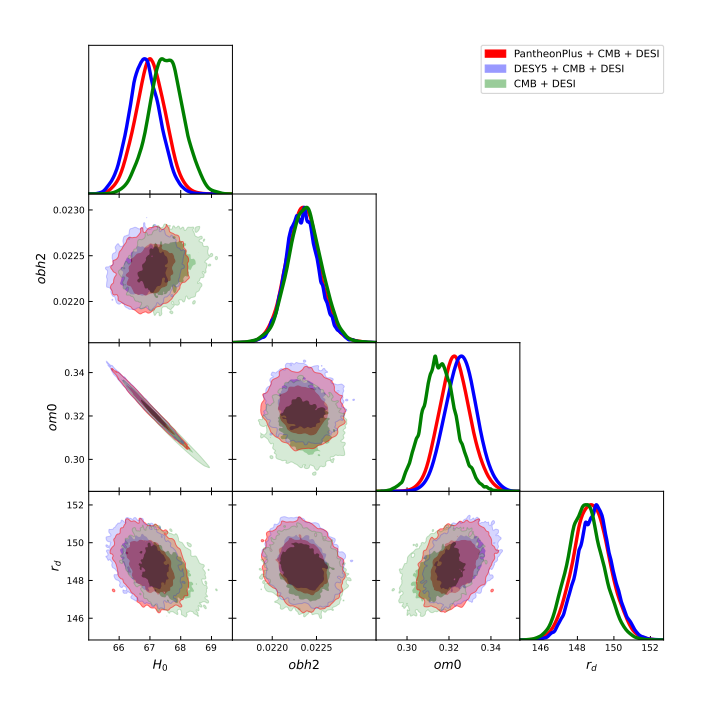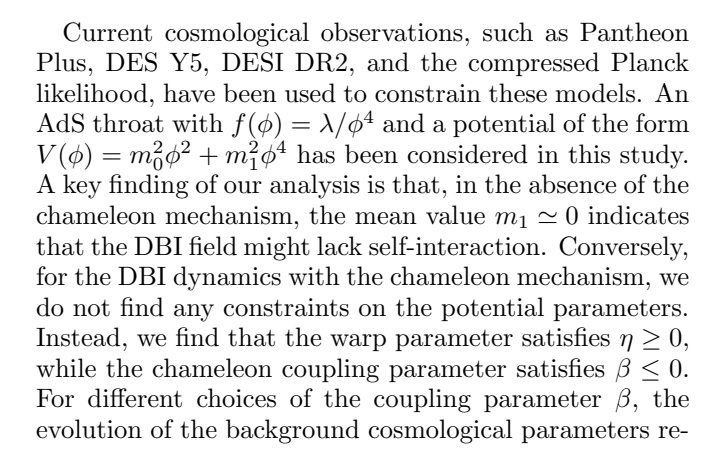

FIG. 5. The plot displays the triangular representation of the 1D and 2D posterior distributions for various cosmological parameters in the DBI model with the chameleon mechanism. The red contours correspond to results from *Pantheon Plus + CMB + DESI*, blue to *DES Y5 + CMB + DESI*, and green to *CMB + DESI*.
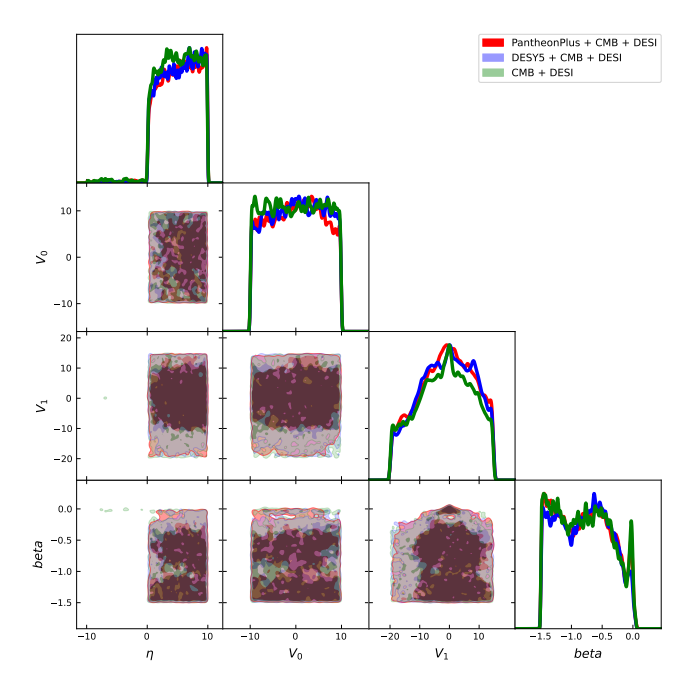

FIG. 6. The plot displays the triangular representation of the 1D and 2D posterior distributions for model parameters η, V_0, V_1 in the DBI model with the chameleon mechanism. The red contours correspond to results from *Pantheon Plus + CMB + DESI*, blue to *DES Y5 + CMB + DESI*, and green to *CMB + DESI*.

Current cosmological observations, such as Pantheon Plus, DES Y5, DESI DR2, and the compressed Planck likelihood, have been used to constrain these models. An AdS throat with $f(\phi) = \lambda/\phi^4$ and a potential of the form $V(\phi) = m_0^2\phi^2 + m_1^2\phi^4$ has been considered in this study. A key finding of our analysis is that, in the absence of the chameleon mechanism, the mean value $m_1 \simeq 0$ indicates that the DBI field might lack self-interaction. Conversely, for the DBI dynamics with the chameleon mechanism, we do not find any constraints on the potential parameters. Instead, we find that the warp parameter satisfies $\eta \geq 0$, while the chameleon coupling parameter satisfies $\beta \leq 0$. For different choices of the coupling parameter β, the evolution of the background cosmological parameters re-

mains identical; however, the equation of state parameter w_{DE} tends to reside more in the quintessence region in the past. We do not observe any phantom barrier crossing for this class of models under the current assumptions for the throat and the potential.

We have also performed a statistical model comparison for these models by computing the ΔAIC relative to the ΛCDM model. These models show moderate to strong evidence in favor of dynamical dark energy and remain viable from an observational point of view, at least at the background level. One could also choose different warped potentials $W(\phi)$ motivated by other string-inspired models for further analysis.
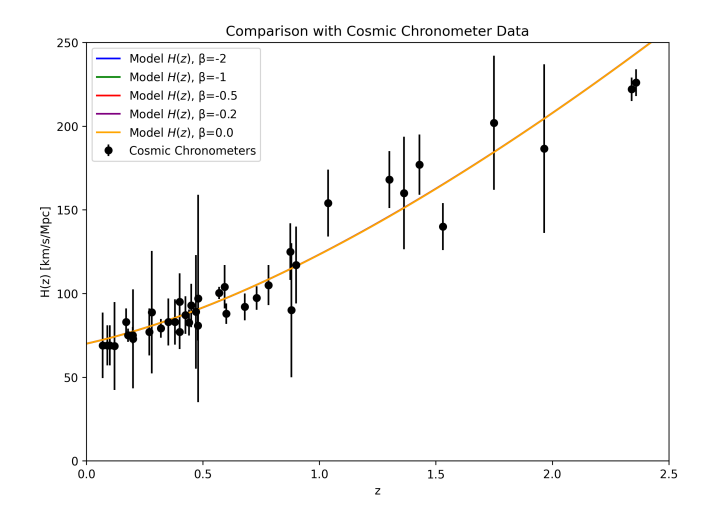
FIG. 7. Evolution of $H(z)$ versus redshift z for the DBI model with the chameleon mechanism. Data points from Cosmic Chronometer datasets are shown for comparison. For the choice of the parameters $m_0 = -0.5, m_1 = 0.05, \eta = -0.5$ with the current value of the $\phi_0 \simeq 1, \dot{\phi}_0 \simeq 0.1$.
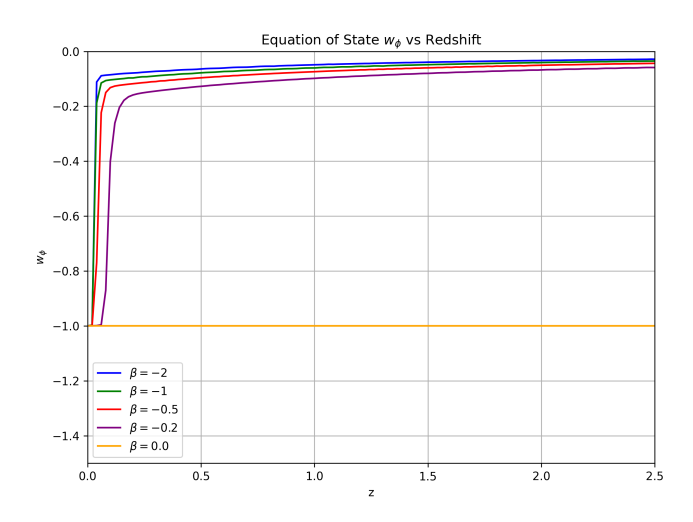

FIG. 8. Evolution of the EOS of the dark energy for the DBI model with the chameleon mechanism for different choices of the chameleon coupling parameter β. For the choice of the parameters $m_0 = -0.5, m_1 = 0.05, \eta = -0.5$ with the current value of the $\phi_0 \simeq 1, \dot{\phi}_0 \simeq 0.1$.

APPENDIX: DERIVATION OF THE FIELD EQUATION

From the action (3), we derived

$$\Gamma' = -\frac{1}{2\Gamma}\left(\frac{T'}{T}\right)\left(\Gamma^2 - 1\right); \qquad (17)$$

$$\frac{\partial \Gamma}{\partial(\partial_\nu \phi)} = \frac{g^{\mu\nu}}{\Gamma}\frac{\partial_\mu \phi}{T}. \qquad (18)$$

Varying the action with respect to the scalar field. The first term of the Euler-Lagrange equation is

$$\frac{\partial}{\partial \phi}\left(\mathcal{L}_{\phi+\mathrm{m}}\right) = \sqrt{-g}\left[-\frac{T'}{2\Gamma}(\Gamma-1)^2 - V'\right] + \mathcal{L}'_\mathrm{m}$$

Then we derive

$$\frac{\partial \mathcal{L}_{\phi+\mathrm{m}}}{\partial(\partial_\nu \phi)} = -\sqrt{-g}\frac{1}{\Gamma}\partial^\nu \phi \qquad (19)$$

$$\nabla_\nu\left[\frac{\partial \mathcal{L}_{\phi+\mathrm{m}}}{\partial(\partial_\nu \phi)}\right] = -\frac{\sqrt{-g}}{\Gamma}\left[\Box^2 \phi - \frac{1}{\Gamma}g^{\rho\nu}(\partial_\rho \phi)(\partial_\nu \Gamma)\right]$$

where $\mathcal{L}_{\phi+\mathrm{m}} \equiv \mathcal{L}_\phi + \mathcal{L}_\mathrm{m}$, $\partial \mathcal{L}_\mathrm{m}/\partial(\partial_\nu \phi) = 0$, $\nabla_\nu \phi = \partial_\nu \phi$, $\nabla_\nu \Gamma^{-1} = -\left(\partial_\nu \Gamma\right)/\Gamma^2$ and $\Box^2 \phi \equiv g^{\mu\nu}\nabla_\mu \nabla_\nu \phi$.

The DBI equation of motion is hence

$$\frac{\Box^2 \phi}{\Gamma} - \frac{T'}{2\Gamma}\left(\Gamma-1\right)^2 - \frac{1}{\Gamma^2}g^{\mu\nu}(\partial_\mu \phi)(\partial_\nu \Gamma) = V' - \frac{\mathcal{L}'_m}{\sqrt{-g}}. \qquad (20)$$

ACKNOWLEDGMENTS

[1] A. G. Riess *et al.* (Supernova Search Team), Astron. J. **116**, 1009 (1998), arXiv:astro-ph/9805201.

[2] N. Aghanim *et al.* (Planck), Astron. Astrophys. **641**, A6 (2020), [Erratum: Astron.Astrophys. 652, C4 (2021)], arXiv:1807.06209 [astro-ph.CO].

[3] T. Padmanabhan, Phys. Rept. **380**, 235 (2003), arXiv:hep-th/0212290.

[4] L. Verde, T. Treu, and A. G. Riess, Nature Astron. **3**, 891 (2019), arXiv:1907.10625 [astro-ph.CO].

[5] S. Alam *et al.* (BOSS), Mon. Not. Roy. Astron. Soc. **470**, 2617 (2017), arXiv:1607.03155 [astro-ph.CO].

[6] S. Joudaki *et al.*, Astron. Astrophys. **638**, L1 (2020), arXiv:1906.09262 [astro-ph.CO].

[7] A. G. Riess *et al.*, Astrophys. J. **826**, 56 (2016), arXiv:1604.01424 [astro-ph.CO].

[8] A. G. Riess, S. Casertano, W. Yuan, L. M. Macri, and D. Scolnic, Astrophys. J. **876**, 85 (2019), arXiv:1903.07603 [astro-ph.CO].

[9] K. C. Wong *et al.* (H0LiCOW), Mon. Not. Roy. Astron. Soc. **498**, 1420 (2020), arXiv:1907.04869 [astro-ph.CO].

[10] W. L. Freedman *et al.*, Astrophys. J. **882**, 34 (2019), arXiv:1907.05922 [astro-ph.CO].

[11] A. G. Adame *et al.* (DESI), JCAP **02**, 021 (2025), arXiv:2404.03002 [astro-ph.CO].

[12] R. Calderon *et al.* (DESI), (2024), arXiv:2405.04216 [astro-ph.CO].

[13] M. Abdul Karim *et al.* (DESI), (2025), arXiv:2503.14738 [astro-ph.CO].

[14] A. G. Adame *et al.* (DESI), (2024), arXiv:2411.12021 [astro-ph.CO].

[15] K. Lodha *et al.* (DESI), (2025), arXiv:2503.14743 [astro-ph.CO].

[16] T. M. C. Abbott *et al.* (DES), Astrophys. J. Lett. **973**, L14 (2024), arXiv:2401.02929 [astro-ph.CO].

[17] E. J. Copeland, M. Sami, and S. Tsujikawa, Int. J. Mod. Phys. **D15**, 1753 (2006), arXiv:hep-th/0603057 [hep-th].

[18] T. Padmanabhan, AIP Conf. Proc. **861**, 179 (2006), arXiv:astro-ph/0603114.

[19] L. Amendola and S. Tsujikawa, *Dark Energy: Theory and Observations* (Cambridge University Press, 2015).

[20] T. Clifton, P. G. Ferreira, A. Padilla, and C. Skordis, Phys. Rept. **513**, 1 (2012), arXiv:1106.2476 [astro-ph.CO].

[21] K. Bamba, S. Capozziello, S. Nojiri, and S. D. Odintsov, Astrophys. Space Sci. **342**, 155 (2012), arXiv:1205.3421 [gr-qc].

[22] N. Roy, S. Goswami, and S. Das, Phys. Dark Univ. **36**, 101037 (2022), arXiv:2201.09306 [astro-ph.CO].

[23] A. Banerjee, H. Cai, L. Heisenberg, E. O. Colgáin, M. M. Sheikh-Jabbari, and T. Yang, Phys. Rev. D **103**, L081305 (2021), arXiv:2006.00244 [astro-ph.CO].

[24] B.-H. Lee, W. Lee, E. O. Colgáin, M. M. Sheikh-Jabbari, and S. Thakur, JCAP **04**, 004 (2022), arXiv:2202.03906 [astro-ph.CO].

[25] C. Krishnan, E. O. Colgáin, M. M. Sheikh-Jabbari, and T. Yang, Phys. Rev. D **103**, 103509 (2021), arXiv:2011.02858 [astro-ph.CO].

[26] S. Das, M. Banerjee, and N. Roy, JCAP **08**, 024 (2019), arXiv:1903.02288 [gr-qc].

[27] A. Joyce, B. Jain, J. Khoury, and M. Trodden, Physics Reports **568**, 1 (2015), arXiv:1407.0059 [astro-ph.CO].

[28] J. Khoury and A. Weltman, Physical Review D **69**, 044026 (2004), arXiv:astro-ph/0309411 [astro-ph].

[29] J. Khoury and A. Weltman, Phys. Rev. Lett. **93**, 171104 (2004).

[30] J. Khoury and A. Weltman, Phys. Rev. D **69**, 044026 (2004).

[31] P. Brax, C. van de Bruck, A.-C. Davis, J. Khoury, and A. Weltman, Phys. Rev. D **70**, 123518 (2004).

[32] D. F. Mota and D. J. Shaw, Phys. Rev. D **75**, 063501 (2007).

[33] C. Burrage and J. Sakstein, Living Rev. Relativ. **21**, 1 (2018).

[34] P. Brax, C. van de Bruck, A.-C. Davis, J. Khoury, and A. Weltman, Phys. Rev. D **70**, 123518 (2004), arXiv:astro-ph/0408415.

[35] A. L. Erickcek, N. Barnaby, C. Burrage, and Z. Huang, Phys. Rev. D **89**, 084074 (2014), arXiv:1310.5149 [astro-ph.CO].

[36] A. L. Erickcek, N. Barnaby, C. Burrage, and Z. Huang, Phys. Rev. Lett. **110**, 171101 (2013), arXiv:1304.0009 [astro-ph.CO].

[37] A. Banerjee, R. K. Jain, and B. M. Mandal, JCAP **2018**, 028 (2018).

[38] T. Damour and A. M. Polyakov, Nucl. Phys. B **423**, 532 (1994).

[39] A. Padilla, E. Platts, D. Stefanyszyn, A. Walters, A. Weltman, and T. Wilson, JCAP **03**, 058 (2016), arXiv:1511.05761 [hep-th].

[40] E. Silverstein and D. Tong, Phys. Rev. D **70**, 103505 (2004), arXiv:hep-th/0310221.

[41] M. Alishahiha, E. Silverstein, and D. Tong, Phys. Rev. D **70**, 123505 (2004), arXiv:hep-th/0404084.

[42] S. Kecskemeti, J. Maiden, G. Shiu, and B. Underwood, JHEP **09**, 076 (2006), hep-th/0605189.

[43] X. Chen, Phys. Rev. D **71**, 063506 (2005), hep-th/0408084.

[44] X. Chen, Phys. Rev. D **72**, 123518 (2005), astro-ph/0507053.

[45] J. Ward, JHEP **12**, 045 (2007), arXiv:0711.0760 [hep-th].

[46] X. Chen, JCAP **12**, 009 (2008), arXiv:0807.3191 [hep-th].

[47] F. Gmeiner and C. White, JCAP **02**, 012 (2008), arXiv:0710.2009 [hep-th].

[48] B. Gumjudpai and J. Ward, Phys. Rev. D **80**, 023528 (2009), arXiv:0904.0472 [astro-ph.CO].

[49] J. E. Lidsey and I. Huston, Journal of Cosmology and Astroparticle Physics **2007**, 002 (2007), arXiv:arXiv:0705.0240 [hep-th].

[50] D. Baumann and L. McAllister, Physical Review D **75**, 123508 (2007), hep-th/0610285.

[51] L. Alabidi and J. E. Lidsey, Physical Review D **78**, 103519 (2008), arXiv:arXiv:0807.2181 [astro-ph].

[52] C. Cheng, Q.-G. Huang, and Y.-Z. Ma, Journal of Cosmology and Astroparticle Physics **2013**, 018 (2013), arXiv:arXiv:1303.4497 [astro-ph.CO].

[53] I. Huston, J. E. Lidsey, S. Thomas, and J. Ward, Journal of Cosmology and Astroparticle Physics **2008**, 016 (2008), arXiv:arXiv:0802.0398 [hep-th].

[54] C. Ahn, C. Kim, and E. V. Linder, Phys. Rev. D **80**, 123016 (2009), arXiv:0909.2637 [astro-ph.CO].

[55] M. R. Garousi, M. Sami, and S. Tsujikawa, Phys. Rev. D **71**, 083005 (2005), arXiv:hep-th/0412002.

[56] J. Martin and M. Yamaguchi, Phys. Rev. D **77**, 123508 (2008), arXiv:0801.3375 [hep-th].

[57] C. Ahn, C. Kim, and E. V. Linder, Phys. Lett. B **684**, 181 (2010), arXiv:0904.3328 [astro-ph.CO].

[58] E. J. Copeland, S. Mizuno, and M. Shaeri, Phys. Rev. D **81**, 123501 (2010), arXiv:1003.2881 [hep-th].

[59] K. Rezazadeh, S. Asadzadeh, K. Fahimi, K. Karami, and A. Mehrabi, Annals Phys. **422**, 168299 (2020), arXiv:2001.07920 [gr-qc].

[60] X. Suo, X. Kang, and H. Shan, Phys. Rev. D **108**, 123506 (2023), arXiv:2307.04394 [astro-ph.CO].

[61] A. R. Liddle and D. H. Lyth, *Cosmological inflation and large scale structure* (2000).

[62] A. Reiss *et al.*, Astron. J **116**, 1009 (1998).

[63] A. G. Riess *et al.* (Supernova Search Team), Astron. J. **116**, 1009 (1998), arXiv:astro-ph/9805201.

[64] D. Scolnic *et al.*, Astrophys. J. **938**, 113 (2022), arXiv:2112.03863 [astro-ph.CO].

[65] A. G. Riess, L. Breuval, W. Yuan, S. Casertano, L. M. Macri, J. B. Bowers, D. Scolnic, T. Cantat-Gaudin, R. I. Anderson, and M. C. Reyes, The Astrophysical Journal **938**, 36 (2022).

[66] D. Brout *et al.*, Astrophys. J. **938**, 110 (2022), arXiv:2202.04077 [astro-ph.CO].

[67] A. G. Riess *et al.*, Astrophys. J. Lett. **934**, L7 (2022), arXiv:2112.04510 [astro-ph.CO].

[68] L. Chen, Q.-G. Huang, and K. Wang, JCAP **02**, 028 (2019), arXiv:1808.05724 [astro-ph.CO].

[69] P. S. Corasaniti and A. Melchiorri, Phys. Rev. D **77**, 103507 (2008), arXiv:0711.4119 [astro-ph].

[70] O. Elgaroy and T. Multamaki, Astron. Astrophys. **471**, 65 (2007), arXiv:astro-ph/0702343.